



Global wind patterns and the vulnerability of wind-dispersed species to climate change

Matthew M. Kling and David D. Ackerly

The resilience of biodiversity in the face of climate change depends on gene flow and range shifts. For diverse wind-dispersed and wind-pollinated organisms, regional wind patterns could either facilitate or hinder these movements, depending on alignment of winds with spatial climate patterns. We map global variation in terrestrial wind regimes, and model how 'windscape' connectivity will shape inbound and outbound dispersal between sites and their predicted future climate analogs. This model predicts that wind-accessible, climatically analogous sites will be scarcer in locations such as the tropics and on the leeward sides of mountain ranges, implying that the wind-dispersed biota in these landscapes may be more vulnerable to future climate change. A case study of *Pinus contorta* illustrates species-specific patterns of predicted genetic rescue and range expansion facilitated by wind. This framework has implications across fields ranging from historical biogeography and landscape genetics to ecological forecasting and conservation planning.

For biodiversity, resilience to climate change eventually requires either range shifts or in situ adaptation¹. Both rely on dispersal. Species survival depends on outbound dispersal to track suitable conditions and resources through range expansion², whereas the adaptation of local populations and ecosystems depends largely on the inbound dispersal of novel genes and species better suited to the new environment³. Already widespread, climate-induced biogeographical shifts are predicted to become a race against time as the pace of climate change accelerates, with major consequences for global biodiversity and human society⁴.

Although some organisms can actively track suitable climates, many passive dispersers are subject to the whim of the winds. Wind is the essential dispersal vector for a substantial fraction of species across all life forms. Wind regimes (speed, direction and directional consistency) help explain the transoceanic dispersal of birds⁵, arthropods⁶, plants⁷ and microorganisms⁸; the regional and local movement of plant pollen and seeds^{9–13} and fungi¹⁴; the landscape genetics of diverse plants^{9,13,15,16} and pathogens¹⁷; and the overland dispersal of aquatic species¹⁸. Wind influences on insect pollinators can even drive directional pollen dispersal in non-wind-pollinated plants¹⁹.

Wind regimes could thus strongly influence the range expansion and gene flow required for climate tracking at landscape to regional scales^{20–22}. Under warming conditions, adaptation and range shifts require the dispersal of genes and species down geographical temperature gradients towards historically cooler sites (for example, towards higher latitudes and elevations)²³. Wind may facilitate this migration in landscapes where it flows strongly from warmer to cooler sites, and hinder it where the flow is from cooler to warmer sites or blows weakly overall^{20,22}. Alignment with precipitation gradients will also be important for many species, but we focus mainly on temperature in this article because future rainfall projections are more heterogeneous and uncertain, and wind has important causal links with temperature gradients.

The direction of currents is a well-established factor in determining the success of climate-driven range shifts in marine systems²⁴, but the corresponding role of wind currents in terrestrial systems has received less attention, in spite of studies that identify

wind direction as a key open question for modelling range shifts^{21,25}. Although studies using wind-speed data have assessed future range-expansion potentials^{21,26,27} and concluded that dispersal could limit future climate responses in many species, we are unaware of studies that account for wind direction or spatial variation in wind regimes. Studies on wind direction's role in historical climate tracking are also scarce, although it has been implicated in shaping local^{28,29} and regional³⁰ climate-driven range expansion. Observations that some wind-dispersed trees and grasses have failed to keep pace with high palaeoclimate velocities^{31,32} and that incomplete range filling is related to seed aerodynamics³³ further suggest that wind conditions can limit range expansion even when climate change is much slower than that predicted for the coming decades.

In this study, we model the predicted global patterns of climate adaptation tailwinds and headwinds. We begin by characterizing the geography of key dispersal-relevant features of local wind regimes. Next, we offer a conceptual introduction that examines climatic drivers of alignment (tailwinds) and misalignment (headwinds) between prevailing winds and temperature gradients. In our main analysis assessing the potential for wind to facilitate climate tracking, we then implement a global 'windscape' connectivity model to compare upwind and downwind dispersal catchments with patterns of shifting climate analogues. Finally, we demonstrate how species-specific wind connectivity modelling can inform predicted patterns of genetic rescue and range expansion under climate change, using lodgepole pine (*Pinus contorta*) as a case study.

A typology of global wind regimes

The geography of wind regimes will determine potential impacts on climate change biogeography. Wind dispersal patterns depend on the long-term distribution of instantaneous wind conditions at a site¹⁰, and these wind regimes can be characterized by three key properties. Average wind speed represents the total wind dispersal potential for a site. Prevailing wind direction represents the expected bearing of wind dispersal to or from a site, quantified as the circular mean of hourly wind angles weighted by wind speed. And wind anisotropy reflects how unidirectional wind dispersal is expected to be for a site, quantified as one minus the circular standard devia-

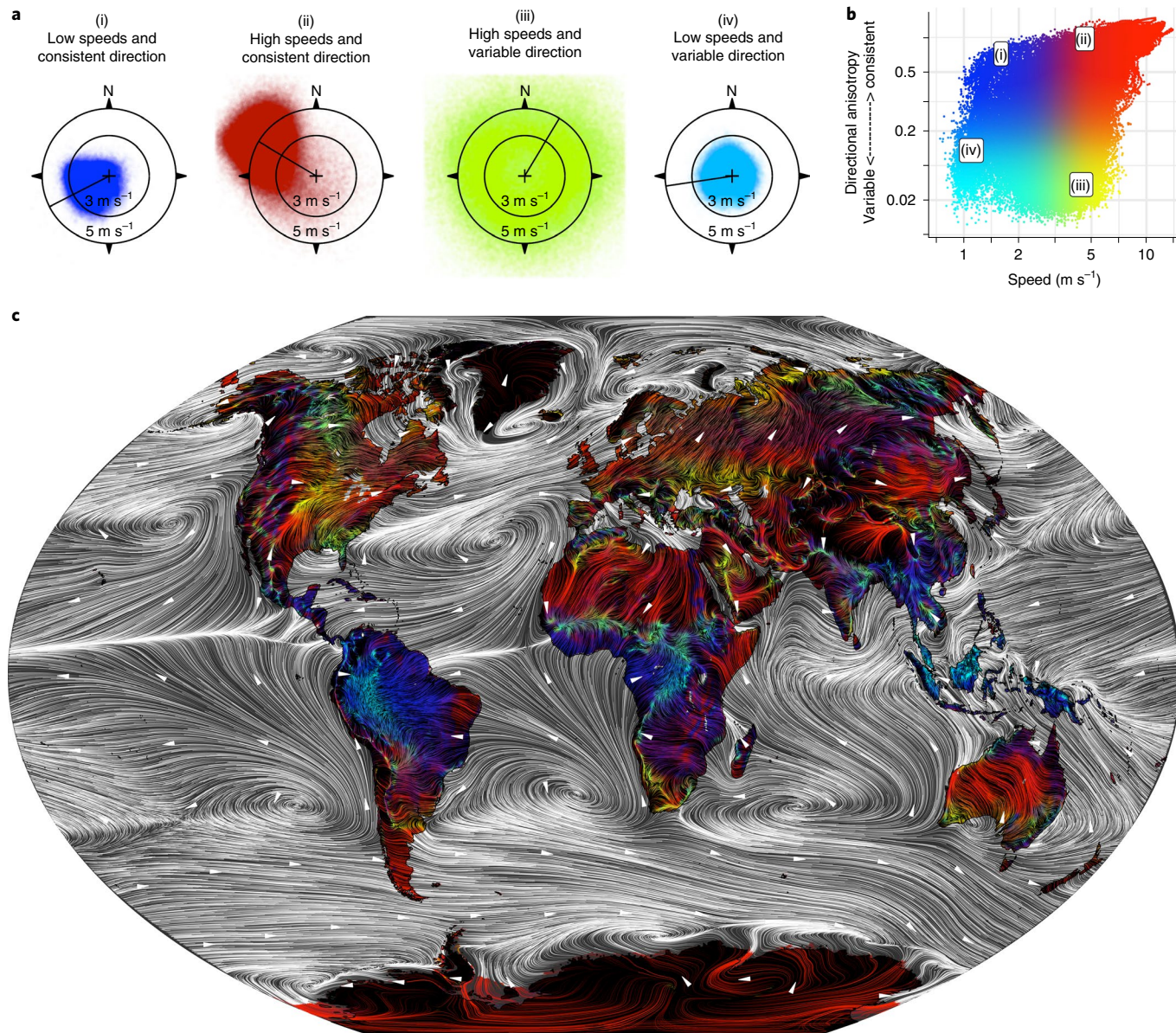


Fig. 1 | Global wind patterns as characterized by three drivers of dispersal: prevailing wind direction, average wind speed and anisotropy. **a**, Examples of local wind regimes; point clouds represent speed and direction for every hour from 1980 to 2009, and radial lines indicate the prevailing direction. **b**, Wind speed and anisotropy across terrestrial grid cells ($r^2=0.25$); the examples in **a** are shown. **c**, Geographical patterns of wind regimes; the prevailing wind direction is indicated by wind paths and arrows, and the speed and anisotropy correspond to the colours in **b**.

tion of hourly wind directions weighted by wind speed. Vertical turbulence also plays a critical role in wind dispersal (Supplementary Appendix 1), although we are unable to assess it in detail due to data and space limitations. Diurnal and seasonal patterns in these factors are also important, depending on the dispersal phenology of individual species¹³.

We characterized global patterns in these wind regime properties using 30 years (1980–2009) of hourly resolution near-surface wind data from the gridded (~35 km pixels) Climate Forecast System Reanalysis (CFSR) dataset³⁴, which we used for all the analyses in this article. Each of the three variables exhibits strong and relatively independent spatial trends (Fig. 1), with important implications for the biogeography of wind dispersal. Globally, the prevailing wind direction is structured in latitudinal bands associated with Hadley, Ferrel and polar atmospheric circulation cells. Equatorial regions have weak westward and equatorward surface flow, which makes

the tropics a relative wind trap (known to sailors as the doldrums); tropical winds tend to be more anisotropic near coasts. At temperate latitudes, winds are stronger and tend to flow eastward and poleward, although the strength and direction are more variable. Polar latitudes exhibit strong anisotropic winds that flow westward and equatorward, although this is more consistent in the Southern Hemisphere. Smaller-scale geography also shapes wind regimes, with wind strength often increasing near coasts and both strength and anisotropy increasing with elevation.

Prevailing wind alignment with temperature gradients

Global wind patterns will influence the direction and speed of movement for wind dispersers in relation to spatial temperature gradients and warming temperatures. Importantly, wind and temperature are mechanistically coupled. The very temperature gradients that biodiversity must traverse to offset climate change are directly responsible

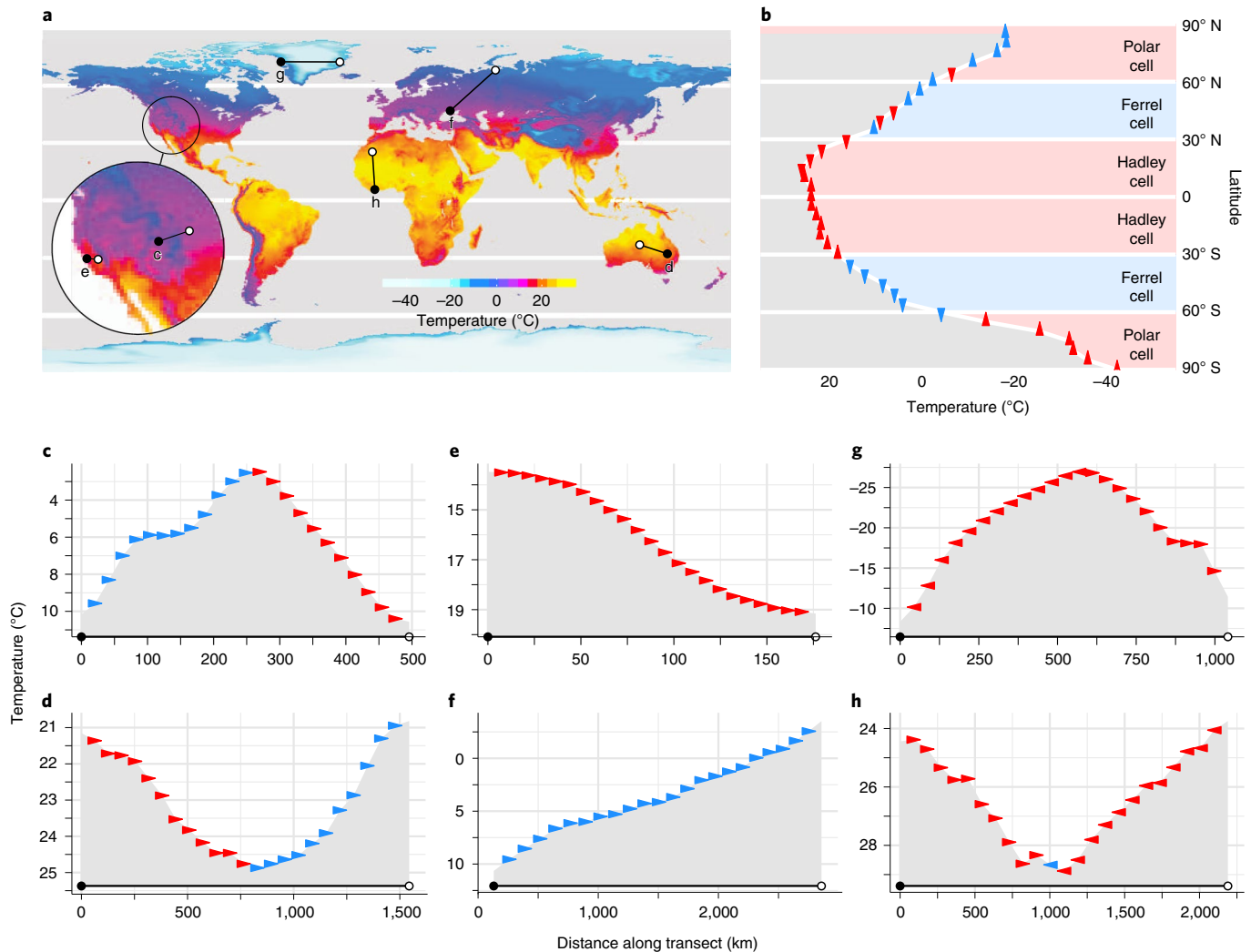


Fig. 2 | Prevailing wind alignment with temperature gradients. **a**, Global temperatures and locations of examples displayed in panels **c–h**. **b–h**,

Characteristic wind-temperature patterns likely to influence climate tracking. Axes show temperature against distance, with the temperature flipped to resemble mountains that are colder at higher elevations. Arrows indicate the prevailing wind direction with respect to the transect—blue for wind that blows towards cooler locations (facilitation) and red where it blows towards warmer locations (hindrance). **b**, Terrestrial meridional winds versus the latitudinal temperature gradient, averaged across 5° latitudinal bins; the coloured rectangles represent hypotheses based on idealized atmospheric cells. **c–h**, Examples of local wind-temperature relationships: transverse mountain wind (**c**), cross-desert wind (**d**), sea breeze (**e**), southwesterly wind (**f**), katabatic wind (**g**) and thermal low (**h**); these transects were selected to roughly parallel prevailing winds.

for generating wind across these landscapes. Generally, the prevailing surface winds tend to flow from cooler towards warmer locations due to the pressure differential between areas of sinking cool air and rising warm air—the opposite direction that genes and species must migrate in a warming world. Although this is a generality, it is also a simplification, and important exceptions exist. In this section we explore general spatial patterns in the alignment ('tailwinds') and misalignment ('headwinds') between prevailing winds and temperature gradients at various geographical scales. We set aside temporal variation in wind speed and direction for this conceptual introduction, and return to it in the subsequent section.

The largest-scale temperature gradient on the planet is latitudinal, and poleward range shifts are a key component of biodiversity migration under climate change. The latitudinal temperature gradient drives equatorward-flowing headwinds in the Hadley and polar cells that cover about two-thirds of the Earth's surface, whereas poleward-flowing tailwinds are the norm in the temperate-latitude Ferrel cells between 30 and 60°N and between 30 and 60°S. Global

data indicate that the mean terrestrial winds follow these expectations across 94% of latitudinal zones outside the Arctic (Fig. 2a,b). Deviations occur in the Arctic and other northern areas where large landmasses interrupt the idealized circulation.

Temperature gradients also drive prevailing winds at regional to landscape scales. Examples include 'thermal lows' pulling wind toward hot deserts, 'katabatic winds' pushing air off of ice caps and high mountains and 'sea breezes' pulling wind from cool waters towards warm landmasses (Fig. 2e,g,h), all of which flow opposite the direction needed to facilitate temperature tracking. In other locations, the prevailing winds flow across landscapes that encompass heterogeneous temperature gradients. Where winds blow across deserts or mountain ranges, they may facilitate migration on one side and hinder it on the other (Fig. 2c,d). The windward side of mountain ranges (generally the west side in temperate regions) will experience tailwinds, which will help move species to higher elevations; on the leeward side, headwinds will push dispersers downhill towards higher temperatures.

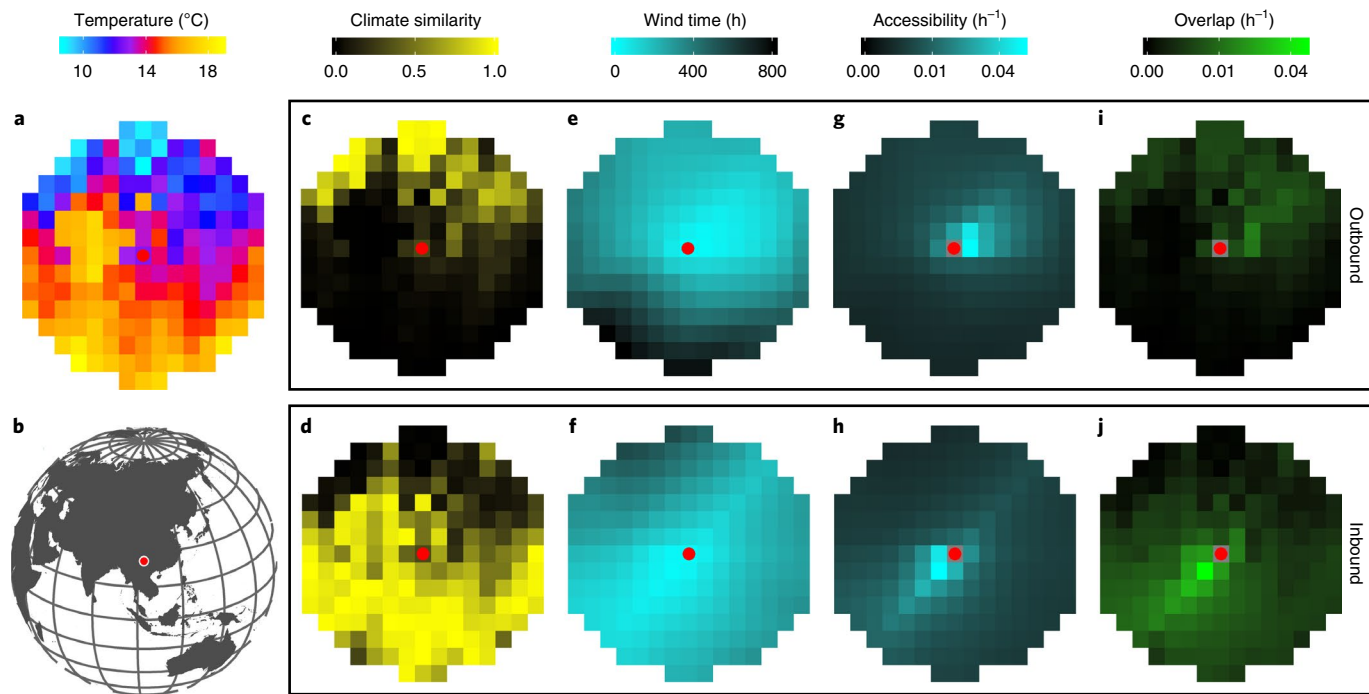


Fig. 3 | Example wind and climate change landscapes for one focal site. **a–d**, For the location in **b**, twentieth century temperature patterns (**a**) combined with future climate change generates patterns of outbound (top row) and inbound (bottom row) climate similarity (**c,d**), which represent emigration and immigration targets for the site. **e–h**, Wind time–distance estimates (**e,f**) that represent the travel time from and to the site are converted into wind accessibility surfaces (**g,h**). **i,j**, The product of wind accessibility and climate similarity is a wind–climate overlap surface, which represents areas that are both accessible and suitable, and are predicted to be the most likely destinations and origins for migrant genes and species associated with this site.

Alignment can be extended to two dimensions by quantifying the angle between the prevailing wind direction and the orientation of the local temperature gradient (Extended Data Fig. 1), and similar metrics for oceanic currents have been shown to explain observed range shifts in marine systems²⁴. However, although prevailing winds offer important insights, winds vary across time and space, and biodiversity must track climates across complex temperature landscapes, which necessitates a more realistic landscape-scale modelling approach.

Upwind and downwind connectivity to analogue climates

Under a given climate change scenario, a focal site will have a particular spatial distribution of climate analogues: outbound analogues represent attractive emigration targets with future climates similar to the site’s historic climate, whereas inbound analogues represent attractive immigration sources with historic climates similar to the focal site’s future condition³⁵ (Fig. 3a–d). (Although originally termed forward and backward analogues³⁵, we find the outbound and inbound terms³⁶ more intuitive and use them here.) In contrast to previous studies, we calculated a continuous metric of inbound or outbound climatic similarity (Supplementary Fig. 5) rather than a discrete classification of analogues. Mapping landscape connectivity to analogue climates has become a major topic of conservation planning, but has focused on actively dispersing terrestrial organisms³⁷. Here we report an analysis of climate change connectivity by wind.

Unlike atmospheric plume models, which represent a single wind-dispersal event associated with a specific weather episode^{38,39}, a dispersal model aimed at capturing long-term biogeographical shifts should integrate over time (which encompasses the long-term distribution of local weather patterns) and over space (which encompasses numerous short dispersal events that link an origin and destination over multiple generations). Landscape connectivity models that represent conductance between neighbouring grid cells

are well-suited to model spatial diffusion, and have been used to study terrestrial dispersal⁴⁰, marine dispersal⁴¹ and wind dispersal using individual wind fields that represent average or instantaneous wind conditions^{7,42}. We extended this landscape wind-connectivity (‘windscape’) approach to allow multidirectional connectivity parameterized using decades-long time series of hourly wind fields. For a given site, this model predicts the relative accessibility of downwind and upwind dispersal landscapes, which represents the potential for outbound emigration and inbound immigration, respectively (Fig. 3e,f).

The expected time for wind to travel between two points, given the full spatiotemporal distribution of wind regimes across a landscape, is measured in wind-hours. Conceptually, this offers a more realistic alternative to geographical distance for predicting the actual time for genes or species to reach a site. As a simple illustration, for a species with a one-year generation time and propagules that spend one hour aloft per dispersal event, the mean spread rate would be one wind-hour per year and the expected years until colonization would equal the wind-hours between sites. Although this example does not reflect the complexity of a species-specific demography, propagule aerodynamics or vertical uplift^{21,39,43} (Supplementary Appendix 1), we propose that relative rates of spread for given genes or species should be roughly proportional to the wind-hours to sites across the region. To validate these model predictions with empirical data and to integrate windscape models with biologically explicit range-expansion models^{39,44} are important areas for future research. For our purposes, we quantify wind accessibility as the inverse of wind-hours between points (Fig. 3g,h). This inverse function resembles the long-tailed wind dispersal kernels used in many studies^{10,21,26}, which reflect the non-linear probability of dispersal at increasing distances.

Comparing a site’s climate analogue and wind-accessibility landscapes (Fig. 3c–h) shows how wind patterns are predicted

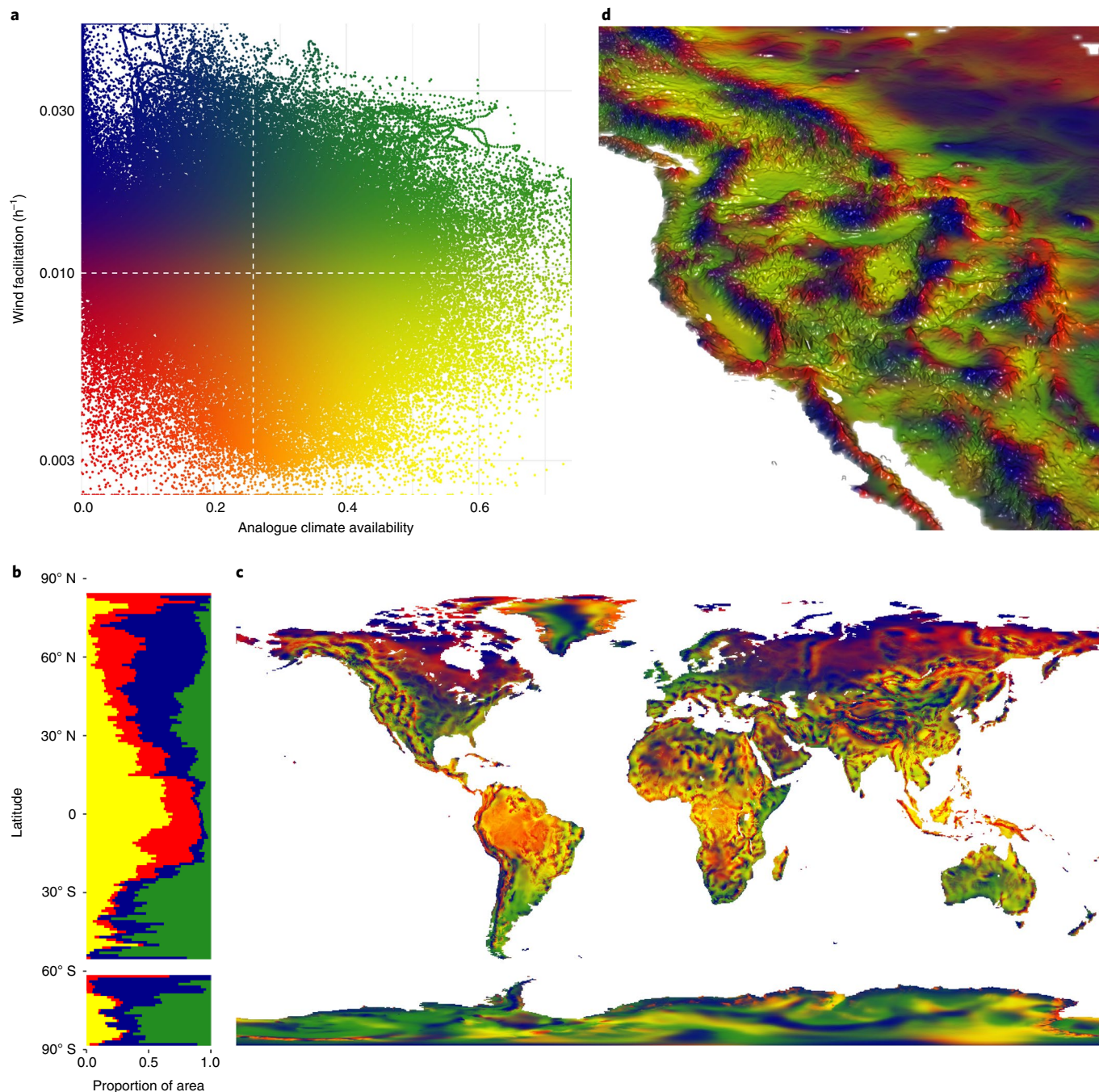


Fig. 4 | Modelled global patterns of downwind accessibility to outbound climate analogues. **a**, Relationship between outbound climate analogue availability and wind facilitation; colours represent combinations of the two variables and extreme outliers were rescaled for visualization. **b**, Latitudinal trends in the relative prevalence of the four categorical combinations of these metrics, which are delineated by the dashed median lines in **a**. **c**, Global geographical patterns in the two metrics. **d**, Regional perspective highlighting the mountain ranges of western North America, where the dominant temperature gradients are elevational and prevailing winds flow towards the east-northeast. Colours in all the panels correspond to those in **a**. See Extended Data Fig. 2 for the inbound results that correspond to these outbound results.

to affect the dispersal accessibility of climatically suitable sites. Wind-climate overlap maps (Fig. 3*i,j*), calculated by multiplying wind accessibility by climatic similarity, represent areas with the highest predicted potential for successful natural migration. Using the 30-year hourly wind data and baseline and future temperature data (1979–2013 versus 2060–2080 under the Representative Concentration Pathway 8.5 emissions scenario), we modelled wind-accessibility and temperature-similarity surfaces for every

terrestrial grid cell in a circular landscape 500 km in diameter, in both the inbound and outbound directions. For each landscape we summarized these surfaces by calculating the mean climate similarity, mean wind accessibility and mean wind-climate overlap across cells. The ratio of overlap to climate similarity gives a normalized metric that we call ‘wind facilitation’, which indicates the degree to which wind is expected to facilitate versus hinder connectivity to the available climate analogues.

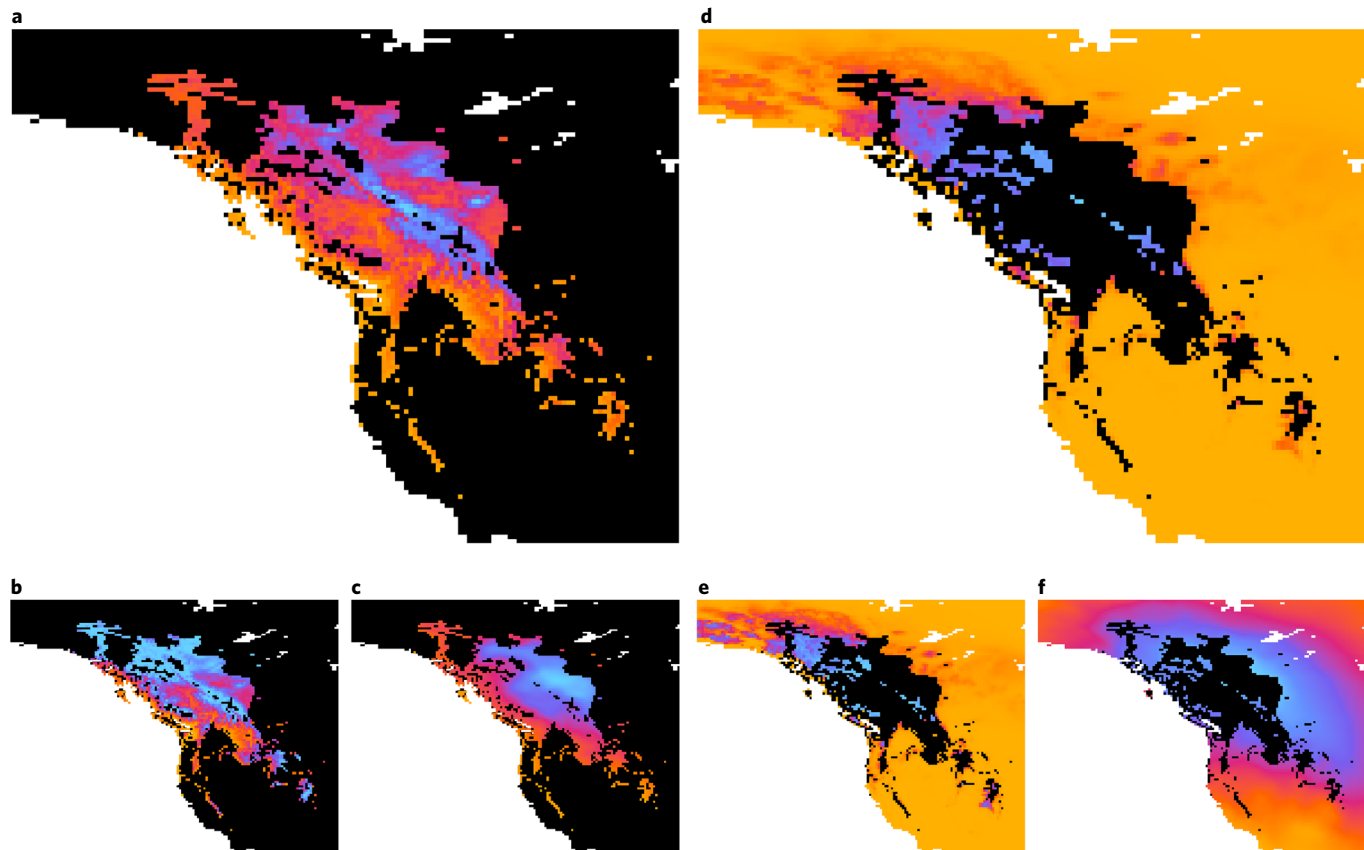


Fig. 5 | Case study of wind connectivity and climate resilience for lodgepole pine in western North America. **a-c**, Potential for wind-mediated genetic rescue (**a**) within the current species range; higher values indicate upwind accessibility to many populations (**b**) with high inbound climate similarity (**c**). **d-f**, Potential for wind-mediated range expansion (**d**), with sites outside the current species range (shown in black) coloured by the product of future suitability (**e**) and wind dispersal pressure (**f**). Gold-red-blue colours represent continua from relative vulnerability to resilience in all the maps; units are h^{-1} , except in **b** and **e**, which are unitless.

Globally, we found that these models predict strong geographical patterns in the wind facilitation of climate tracking. Facilitation is higher in temperate latitudes and on the windward sides of mountain ranges (Fig. 4 and Extended Data Figs. 2–4). Relationships between facilitation and coastal or elevational gradients are also prominent in some regions, and often differ between the inbound and outbound directions; for example, along the immediate eastern coast of North America, winds that flow offshore are expected to facilitate inbound migration from warmer inland areas, but hinder outbound migration. For cases in which climate analogues are abundant but facilitation is low, wind could hinder range shifts either because it blows in the wrong direction (headwinds) or because it blows too weakly, syndromes that exhibit strong global patterns (Extended Data Fig. 5).

Patterns in the underlying wind and climate change components are also notable. Wind-dispersal potential itself is much higher at high absolute latitudes, and exhibits strong but regionally variable relationships with elevation (Extended Data Fig. 6). Prior studies hypothesized that the latitudinal wind-speed gradient may be responsible for the higher prevalence of wind-pollinated and wind-dispersed plants at higher latitudes⁴⁵. Whether this is due to evolution towards wind dispersal at higher latitudes or to greater colonization of temperate regions by wind dispersers, it illustrates the potentially profound role of global wind geography in shaping biodiversity patterns. It also means our results will be relevant to a larger fraction of the flora in temperate than in tropical areas.

Contrasts between inbound and outbound climate tracking have important ecological and conservation implications. The outbound direction emphasizes the resilience of the taxonomic or genetic diversity currently present at a site, whereas the inbound direction emphasizes the site's ability to sustain diversity and function through immigration of new genes and species; the concepts are therefore most relevant to species-based versus place-based conservation perspectives, respectively^{35,46}. Where inbound and outbound migration are balanced, temporal turnover is expected, in which genes and species replace each other as all move up a common gradient; where they diverge, transient ecological states of extinction debt or immigration credit may persist for extended periods of time⁴⁷. We found weak correlations between wind-analogue overlap area in the outbound versus inbound directions (Extended Data Fig. 2), which suggests that ecological disequilibria may become widespread, and that the areas of greatest conservation concern may differ by management perspective. This result is driven not by wind, but by climate analogue availability; for example, outbound availability is higher than inbound at low elevations, but this reverses at high elevations (Extended Data Fig. 7) and the two metrics exhibit a triangular relationship in which they are never both high (Extended Data Fig. 2d). Such patterns are broadly consequential for both wind- and non-wind-dispersed taxa^{35,46,48}.

We stress that these model predictions are hypotheses that should be tested and refined by future empirical work. We expect wind-speed-based connectivity to correlate positively with dispersal potential on average, but there is substantial uncertainty in this

average, and in the translation from relative to absolute measures of wind accessibility, due to the simple nature of our model. There will also be major variation around the average in the application to different species. In Supplementary Appendix 1 we discuss a number of these uncertainties in more detail, and present a set of sensitivity analyses (Supplementary Figs. 1–7) related to different model assumptions and parameters. Notably, our overall conclusions are relatively robust under a range of alternative parameterizations. Beyond dispersal dynamics, our focus on the mean annual temperature for the climate change component also adds uncertainty. Sensitivity analyses indicate that wind facilitation patterns based on seasonal temperature and annual precipitation are similar to those for mean annual temperature, whereas patterns based on seasonal precipitation differ substantially (Supplementary Fig. 6); our results will therefore be less relevant for species whose climate suitability is highly dependent on precipitation seasonality.

Case study of genetic rescue and range expansion in lodgepole pine

Windscape models can be used to assess the potential for genetic rescue and species range expansion for particular focal species, incorporating additional geographical and biological features. We demonstrate this for lodgepole pine (*P. contorta*), a wind-dispersed, wind-pollinated tree of major ecological and commercial importance in western North America. In this species, pollination occurs in late spring and seed release occurs mainly during late summer and autumn⁴⁹; we thus used wind data from these seasons for the gene flow and range-expansion models, respectively. Also, as pine seeds (unlike pollen) probably have higher rates of abscission and uplift under higher wind speeds (Supplementary Appendix 1), we modelled connectivity for range expansion and gene flow as quadratic and linear functions of wind speed, respectively.

Genetic rescue entails gene flow that bolsters a population's declining fitness under warming climates^{50,51}. We modelled this by calculating inbound wind conductance between all the population pairs within the current species range, and comparing their current and predicted future climates in light of published population-level thermal performance curves^{52,53}, which reflect patterns of niche breadth and local adaptation in *P. contorta*. The highest potential for genetic rescue occurs in populations in northeastern portions of the species range that are downwind from numerous substantially warmer populations; greater vulnerability is predicted for populations near the warm edge of the range and for populations in cooler areas but with poor inbound wind connectivity to warmer populations (Fig. 5a–c). Although long generation times limit evolutionary rates, these results may reflect not just future gene flow, but also existing *in situ* adaptive genetic variation from historic gene flow.

To assess the role of winds in range-expansion potential, we used an environmental niche model based on multiple temperature and precipitation variables to predict future suitability across the region, and modelled outbound wind connectivity from every location in the current range to the surrounding region. Sites with a high future suitability that are downwind from many occupied sites are most likely to be colonized, whereas areas with low suitability or poor wind connectivity to the current range have a lower predicted colonization potential (Fig. 5d–f). For lodgepole pine, most newly suitable habitat is predicted to be northwest of the current species range, whereas wind-dispersal potential is predicted to be strongest towards the east. This suggests that wind is less likely to facilitate a rapid natural expansion to the northwest, whereas higher-elevation areas encircled by the species range are more likely to be both suitable and wind accessible.

Discussion

In this study, we explored the possibility that global wind patterns may influence the ability of wind-dispersed genes and species to

keep up with climate change. Combining a novel wind-connectivity model with future temperature data, we generated hypotheses about the sorts of patterns that could result from this phenomenon, such as the facilitation of upward elevational migration on the windward mountain slopes and poleward migration in temperate regions. The wind-dispersed biota in these regions may be able to naturally adapt to future temperature increases through genetic rescue and range shifts, whereas areas characterized by wind hindrance may have less capacity to adapt and could be higher priorities for management intervention. At the level of the individual species range, we also projected how wind could influence range expansion and adaptive gene flow, and so facilitate climate change resilience in some landscapes but hinder it elsewhere. Testing these hypotheses with empirical data and refining windscape-modelling methods to increase their biological and meteorological realism are important priorities for future studies. If winds do shape future climate vulnerability patterns as predicted here, it could have profound ecological consequences, not just for wind-dispersed species, but also indirectly for entire ecosystems in which they play important roles, such as temperate forests with the majority of trees are wind-dispersed, wind pollinated or both. Our results are also relevant in cases when the goal is to prevent range expansion, such as for pathogens and invasive species.

Although there is a long history of wind-dispersal modelling, the role of wind geography has been underexplored at the landscape-to-regional scales important for the dynamics of species ranges, metacommunities and population genetics, including responses to climate change. The connectivity modelling approach we utilize here helps address this gap and offers hypotheses about the relative ease of wind dispersal between locations. Here we combined these predictions with data on future climate change to predict where wind may facilitate versus hinder climate adaptation. Windscape models also generate predictions about historical patterns—predictions that will be useful to both improve dispersal models and climate vulnerability forecasts and also to understand historical ecological patterns. Windscape models hold promise for integration with climate-change-focused studies on simulated range expansion, incomplete range filling, palaeoclimatic range shifts and long-distance gene flow, as well as diverse areas of spatial ecology and biogeography not explicitly connected to climate change.

Online content

Any methods, additional references, Nature Research reporting summaries, source data, extended data, supplementary information, acknowledgements, peer review information; details of author contributions and competing interests; and statements of data and code availability are available at <https://doi.org/10.1038/s41558-020-0848-3>.

Received: 3 September 2019; Accepted: 15 June 2020;

Published online: 20 July 2020

References

1. Bellard, C., Bertelsmeier, C., Leadley, P., Thuiller, W. & Courchamp, F. Impacts of climate change on the future of biodiversity. *Ecol. Lett.* **15**, 365–377 (2012).
2. Hampe, A. Plants on the move: the role of seed dispersal and initial population establishment for climate-driven range expansions. *Acta Oecol.* **37**, 666–673 (2011).
3. Kremer, A. et al. Long-distance gene flow and adaptation of forest trees to rapid climate change. *Ecol. Lett.* **15**, 378–392 (2012).
4. Pecl, G. T. et al. Biodiversity redistribution under climate change: impacts on ecosystems and human well-being. *Science* **355**, eaai9214 (2017).
5. Felicísimo, Á. M., Muñoz, J. & González-Solis, J. Ocean surface winds drive dynamics of transoceanic aerial movements. *PLoS ONE* **3**, e2928 (2008).
6. Gillespie, R. G. et al. Long-distance dispersal: a framework for hypothesis testing. *Trends Ecol. Evol.* **27**, 47–56 (2012).
7. Muñoz, J., Felicísimo, Á. M., Cabezas, F., Burgaz, A. R. & Martínez, I. Wind as a long-distance dispersal vehicle in the Southern Hemisphere. *Science* **304**, 1144–1147 (2004).

8. Smith, D. J. et al. Intercontinental dispersal of bacteria and archaea by transpacific winds. *Appl. Environ. Microbiol.* **79**, 1134–1139 (2013).
9. Austerlitz, F., Dutech, C., Smouse, P. E., Davis, F. & Sork, V. L. Estimating anisotropic pollen dispersal: a case study in *Quercus lobata*. *Heredity* **99**, 193–204 (2007).
10. Bullock, J. M. & Clarke, R. T. Long distance seed dispersal by wind: measuring and modelling the tail of the curve. *Oecologia* **124**, 506–521 (2000).
11. Gassmann, M. I. & Pérez, C. F. Trajectories associated to regional and extra-regional pollen transport in the southeast of Buenos Aires province, Mar del Plata (Argentina). *Int. J. Biometeorol.* **50**, 280–291 (2006).
12. Skarpaas, O. & Shea, K. Dispersal patterns, dispersal mechanisms, and invasion wave speeds for invasive thistles. *Am. Naturalist* **170**, 421–430 (2007).
13. Wang, Z. F. et al. Pollen and seed flow under different predominant winds in wind-pollinated and wind-dispersed species *Engelhardia roxburghiana*. *Tree Genet. Genomes* **12**, 19 (2016).
14. Soubeyrand, S., Enjalbert, J., Sanchez, A. & Sache, I. Anisotropy, in density and in distance, of the dispersal of yellow rust of wheat: experiments in large field plots and estimation. *Phytopathology* **97**, 1315–1324 (2007).
15. Born, C., le Roux, P. C., Spohr, C., McGeoch, M. A. & van Vuuren, B. J. Plant dispersal in the sub-Antarctic inferred from anisotropic genetic structure. *Mol. Ecol.* **21**, 184–194 (2012).
16. Geremew, A., Woldemariam, M. G., Kefalew, A., Stiers, I. & Triest, L. Isotropic and anisotropic processes influence fine-scale spatial genetic structure of a keystone tropical plant. *AoB Plants* **10**, plx076 (2018).
17. Brown, J. K. & Hovmöller, M. S. Aerial dispersal of pathogens on the global and continental scales and its impact on plant disease. *Science* **297**, 537–541 (2002).
18. Vanschoenwinkel, B., Gielen, S., Seaman, M. & Brendonck, L. Any way the wind blows—frequent wind dispersal drives species sorting in ephemeral aquatic communities. *Oikos* **117**, 125–134 (2008).
19. Ahmed, S., Compton, S. G., Butlin, R. K. & Gilman, P. M. Wind-borne insects mediate directional pollen transfer between desert fig trees 160 kilometers apart. *Proc. Natl Acad. Sci. USA* **106**, 20342–20347 (2009).
20. Larson-Johnson, K. Field observations of *Carpinus* (Betulaceae) demonstrate high dispersal asymmetry and inform migration simulations with implications for times of rapid climate change. *Int. J. Plant Sci.* **177**, 389–399 (2016).
21. Nathan, R. et al. Spread of North American wind-dispersed trees in future environments. *Ecol. Lett.* **14**, 211–219 (2011).
22. Sorte, C. J. Predicting persistence in a changing climate: flow direction and limitations to redistribution. *Oikos* **122**, 161–170 (2013).
23. Loarie, S. R. et al. The velocity of climate change. *Nature* **462**, 1052–1055 (2009).
24. Molinos, J. G., Burrows, M. T. & Poloczanska, E. S. Ocean currents modify the coupling between climate change and biogeographical shifts. *Sci. Rep.* **7**, 1332 (2017).
25. Higgins, S. I. et al. Forecasting plant migration rates: managing uncertainty for risk assessment. *J. Ecol.* **91**, 341–347 (2003).
26. Bullock, J. M. et al. Modelling spread of British wind-dispersed plants under future wind speeds in a changing climate. *J. Ecol.* **100**, 104–115 (2012).
27. Kuparinen, A., Katul, G., Nathan, R. & Schurr, F. M. Increases in air temperature can promote wind-driven dispersal and spread of plants. *Proc. R. Soc. B* **276**, 3081–3087 (2009).
28. Davis, H. G., Taylor, C. M., Lambrinos, J. G. & Strong, D. R. Pollen limitation causes an Allee effect in a wind-pollinated invasive grass (*Spartina alterniflora*). *Proc. Natl Acad. Sci. USA* **101**, 13804–13807 (2004).
29. Dullinger, S., Dirnböck, T. & Grabbherr, G. Patterns of shrub invasion into high mountain grasslands of the Northern Calcareous Alps, Austria. *Arct. Antarct. Alp. Res.* **35**, 434–441 (2003).
30. Payette, S. The range limit of boreal tree species in Québec-Labrador: an ecological and palaeoecological interpretation. *Rev. Palaeobot. Palynol.* **79**, 7–30 (1993).
31. Sandel, B., Monnet, A. C., Govaerts, R. & Vorontsova, M. Late Quaternary climate stability and the origins and future of global grass endemism. *Ann. Bot.* **119**, 279–288 (2016).
32. Svensson, J. C. & Skov, F. Could the tree diversity pattern in Europe be generated by postglacial dispersal limitation? *Ecol. Lett.* **10**, 453–460 (2007).
33. Schurr, F. M. et al. Colonization and persistence ability explain the extent to which plant species fill their potential range. *Glob. Ecol. Biogeogr.* **16**, 449–459 (2007).
34. Saha, S. et al. The NCEP Climate Forecast System Reanalysis. *Bull. Am. Meteorol. Soc.* **91**, 1015–1058 (2010).
35. Hamann, A., Roberts, D. R., Barber, Q. E., Carroll, C. & Nielsen, S. E. Velocity of climate change algorithms for guiding conservation and management. *Glob. Change Biol.* **21**, 997–1004 (2015).
36. Kling, M. M., Auer, S. L., Comer, P. J., Ackerly, D. D. & Hamilton, H. Multiple axes of ecological vulnerability to climate change. *Glob. Change Biol.* **26**, 2798–2813 (2020).
37. Keeley, A. T. et al. New concepts, models, and assessments of climate-wise connectivity. *Environ. Res. Lett.* **13**, 073002 (2018).
38. Savage, D., Barbetti, M. J., MacLeod, W. J., Salam, M. U. & Renton, M. Timing of propagule release significantly alters the deposition area of resulting aerial dispersal. *Diversity Distrib.* **16**, 288–299 (2010).
39. Nathan, R. et al. Long-distance biological transport processes through the air: can nature's complexity be unfolded in silico? *Divers. Distrib.* **11**, 131–137 (2005).
40. Zeller, K. A., McGarigal, K. & Whiteley, A. R. Estimating landscape resistance to movement: a review. *Landscape Ecol.* **27**, 777–797 (2012).
41. Tremblay, E. A., Halpin, P. N., Urban, D. L. & Pratson, L. F. Modeling population connectivity by ocean currents, a graph-theoretic approach for marine conservation. *Landscape Ecol.* **23**, 19–36 (2008).
42. Fernández-López, J. & Schliep, K. rWind: download, edit and include wind data in ecological and evolutionary analysis. *Ecography* **42**, 804–810 (2019).
43. Thompson, S. & Katul, G. Plant propagation fronts and wind dispersal: an analytical model to upscale from seconds to decades using superstatistics. *Am. Naturalist* **171**, 468–479 (2008).
44. Savage, D., Barbetti, M. J., MacLeod, W. J., Salam, M. U. & Renton, M. Can mechanistically parameterised, anisotropic dispersal kernels provide a reliable estimate of wind-assisted dispersal? *Ecol. Model.* **222**, 1673–1682 (2011).
45. Regal, P. J. Pollination by wind and animals: ecology of geographic patterns. *Annu. Rev. Ecol. Syst.* **13**, 497–524 (1982).
46. Carroll, C., Lawler, J. J., Roberts, D. R. & Hamann, A. Biotic and climatic velocity identify contrasting areas of vulnerability to climate change. *PLoS ONE* **10**, e0140486 (2015).
47. Jackson, S. T. & Sax, D. F. Balancing biodiversity in a changing environment: extinction debt, immigration credit and species turnover. *Trends Ecol. Evol.* **25**, 153–160 (2010).
48. Ackerly, D. D. et al. The geography of climate change: implications for conservation biogeography. *Divers. Distrib.* **16**, 476–487 (2010).
49. Owens, J. N. *The Reproductive Biology of Lodgepole Pine* Extension Note 07 (Forest Genetics Council of British Columbia, 2006).
50. Bontrager, M. & Angert, A. L. Gene flow improves fitness at a range edge under climate change. *Evol. Lett.* **3**, 55–68 (2019).
51. Sexton, J. P., Strauss, S. Y. & Rice, K. J. Gene flow increases fitness at the warm edge of a species' range. *Proc. Natl Acad. Sci. USA* **108**, 11704–11709 (2011).
52. Rehfeldt, G. E., Ying, C. C., Spittlehouse, D. L. & Hamilton, D. A. Jr Genetic responses to climate in *Pinus contorta*: niche breadth, climate change, and reforestation. *Ecol. Monogr.* **69**, 375–407 (1999).
53. Wang, T., O'Neill, G. A. & Aitken, S. N. Integrating environmental and genetic effects to predict responses of tree populations to climate. *Ecol. Appl.* **20**, 153–163 (2010).

Publisher's note Springer Nature remains neutral with regard to jurisdictional claims in published maps and institutional affiliations.

© The Author(s), under exclusive licence to Springer Nature Limited 2020

Methods

Climate data. Our analysis is based on wind data from the CFSR³⁴, a gridded global climate reanalysis dataset with a temporal resolution of 1 h and a spatial resolution of ~35 km. The CFSR is a weather model continually parameterized with empirical hourly data from meteorological stations worldwide, and is considered the best-available representation of the actual state of the Earth's atmosphere over recent decades³⁴. We used hourly mean near-surface (10 m) zonal (u , that is the east–west component) and meridional (v , that is the north–south component) wind speeds from 1980 through 2009 ($n = 262,800$ hourly time steps), which we converted from the native Gaussian grid format into latitude–longitude raster grids with a spatial resolution of 0.312°. Data from other atmospheric heights were also compared with winds 10 m above ground in a sensitivity analysis (Supplementary Fig. 2) and found to yield similar global patterns of wind facilitation.

We used gridded climate surfaces for historical (1979–2013 mean) and projected future (2060–2080 mean) time periods from the CHELSA (climatologies at high resolution for the Earth's land surface areas) downsampled climate dataset⁵⁴, aggregated to the CFSR spatial grid. Future data were the mean of an ensemble of ten Coupled Model Intercomparison Project 5 (CMIP5) models (ACCESS1-0, CESM1-BGC, CESM1-CAM5, CMCC-CM, FIO-ESM, GISS-E2-H, inmcm4, IPSL-CM5A-MR, MIROC5, MPI-ESM-MR) for the Representative Concentration Pathway 8.5 emissions scenario. The primary analyses were done using mean annual temperature, with the exception of the *P. contorta* species distribution model, for which we used a total of 12 climate variables (monthly minimum and maximum temperatures and monthly total precipitation for January, April, July and October).

Wind regimes. To characterize the wind regime of each grid cell, we calculated three summary statistics based on the 30-year time series of hourly u and v wind speeds: mean speed, prevailing direction and anisotropy. Hourly u and v components were first converted into hourly speed ($\sqrt{(u^2 + v^2)}$) and direction ($\arctan(v/u)$). The mean speed was calculated as the average of the hourly speeds. The prevailing direction was calculated as the circular mean of the hourly direction, weighted by speed. Anisotropy was calculated as 1 minus the circular standard deviation of the hourly wind direction, weighted by speed, and can theoretically range from 0 for a location with a perfectly uniform circular distribution to 1 for a location with no variation in wind direction.

Wind–temperature alignment. To illustrate the spatial patterns of climate change headwinds and tailwinds, we compared local prevailing wind direction with local temperature gradients. For a one-dimensional analysis along a transect across a sequence of grid cells (Fig. 2c–h) or along a global sequence of latitudinal bins (Fig. 2b), the wind–temperature alignment at each point is a binary variable that indicates whether the sign of the prevailing wind matches the sign of the temperature gradient. The wind sign at each point is positive if the angle between the prevailing local wind bearing and the transect bearing is acute, or negative if it is obtuse; this is most relevant if transects run parallel to the prevailing winds, and we chose examples accordingly (Fig. 2). The sign of the temperature gradient at each point is positive if its leading neighbour is colder than its lagging neighbour, and negative if it is warmer.

For a two-dimensional analysis (Extended Data Fig. 1), alignment is an angle between 0 and 180° that represents the difference between the prevailing wind direction and the angle of the local temperature gradient. This temperature gradient angle is calculated by fitting a plane across the temperature values for a focal cell and its eight closest neighbours, as described by Dobrowski et al.⁵⁵.

Wind connectivity. We used graph-theory-based methods from landscape connectivity modelling to estimate wind connectivity between pairs of grid cells. In our model, each grid cell ('node') in a global graph has 16 connections ('edges'), which include an inbound and outbound connection with each of its 8 'queen' neighbours. Conductance along each of these edges represents the frequency and speed of wind flowing in that direction, averaged over the long-term distribution of hourly wind conditions at both nodes. Note that although our main analysis uses wind speed directly in these conductance calculations, wind speeds can also be transformed first to represent the non-linear relationships between wind speed and dispersal expected for particular species, as is discussed in Supplementary Appendix 1, implemented for seed dispersal in the *P. contorta* case study and explored in Supplementary Fig. 3.

For a given hourly timestep at a given node, conductance was allocated to four edges based on wind speed and direction at that node. A wind blowing towards the east–northeast contributes conductance to its eastern and northeastern neighbours, and also conductance from its western and southwestern neighbours. Conductance (s^{-1}) is calculated as wind speed ($m s^{-1}$) divided by intercell distance (m), and is allocated across these edges in proportion to the difference between the wind direction and the bearing to the centre of each neighbouring cell. For example, a wind blowing at 81° is 80% of the way between its northeastern neighbour at 45° and its eastern neighbour at 90°, and would thus contribute 80% of its speed to the former edge and 20% to the latter. Angles and distances between nodes were calculated to reflect the distortion of a square latitude–longitude grid wrapped on a geodesic spheroid, and edge-conductance values were averaged over many

hourly wind values to develop a final global connectivity graph. As our focus was on terrestrial organisms, we downweighted conductance over water by 90%, which makes dispersing over large lakes and oceans difficult but not impossible. Finally, edge-conductance values were inverted to derive resistance (s) to represent the expected wind travel time along every edge of the graph, and the results were converted into units of hours for ease of interpretation.

Based on this connectivity graph, cumulative resistance between a given pair of grid cells can be calculated in either direction using a variety of algorithms from graph theory; we used a least-cost-path algorithm (implemented in the R package gdistance⁵⁶), which identifies cumulative travel time along the shortest path that connects two locations (Fig. 3e–f). Our focal metric, wind accessibility, is calculated as the inverse of cumulative wind-hours (Fig. 3g,h). Alternatives to this inverse function for wind accessibility yield similar results, which indicates that our qualitative results are not especially sensitive to this modelling choice (Supplementary Fig. 4). For every terrestrial grid cell, we calculated wind accessibility both to and from all the other terrestrial cells within 250 km, which generates a distinct upwind and downwind accessibility surface or 'windshed' that represents the ease of inbound or outbound wind dispersal, respectively. A sensitivity analysis using alternative landscape sizes in the range 50–2,500 km in radius (Supplementary Fig. 7) indicates that the final modelled wind facilitation patterns are relatively insensitive to the size of the landscape considered.

Climate similarity. In addition to inbound and outbound wind accessibility surfaces, we calculated inbound and outbound climate similarity surfaces for each grid cell across the same 250-km-radius landscapes. For a given grid cell, we calculated the difference between its historical climate and the future climates of all cells across the landscape (outbound) and also between its future climate and the historical climates of all cells across the landscape (inbound). 'Climate' here refers to mean annual temperature, although we compared this with alternative climate variables in a sensitivity analysis (Supplementary Fig. 6). Climate differences were converted to unitless similarity values between 0 and 1 (Fig. 3c,d), based on a Gaussian decay function with a standard deviation of $\sigma = 2^\circ\text{C}$. This σ value yields a similarity function (Supplementary Fig. 5) that falls off steeply beyond 1.5°C , a range considered to be a critical threshold for many terrestrial ecosystems^{57,58}. Under this function, absolute temperature differences of 0, 1, 2, 3 and 4°C translate to similarity values of 1.00, 0.88, 0.61, 0.32, 0.14 and 0.04, respectively. A sensitivity analysis to evaluate alternative forms and breadths of the climate similarity function (Supplementary Fig. 5) found that the predicted global wind facilitation patterns are not highly sensitive to this modelling choice.

Wind facilitation. Climate similarity surfaces were multiplied by wind accessibility surfaces to represent areas of overlap that are accessible and climatically similar to a given grid cell (Fig. 3i,j). This yielded a total of six surfaces associated with each grid cell: wind accessibility, climate similarity and wind–climate overlap, each in the inbound and outbound directions. Next, we calculated the mean value across each of these surfaces to derive landscape summaries, which gave the amounts of wind-accessible area, analogue climate availability and wind–climate overlap area in the moving window around each grid cell. Finally, we divided the mean wind–climate overlap for each cell by its mean climate analogue availability to calculate the proportion of climatically similar area that is accessible by wind, a variable we call outbound or inbound wind facilitation, which indicates the extent to which wind is projected to facilitate or hinder the dispersal of genes and species to or from suitable sites.

We also characterized the degree to which cells fall into one of four relative wind-facilitation syndromes based on how they ranked globally in terms of climate analogue availability, wind facilitation and windshed anisotropy across their surrounding landscapes. Sites were considered 'climate limited' if they ranked low for climate availability. Non-climate-limited sites were considered wind facilitated if they ranked high for the facilitation ratio, or wind hindered otherwise. Wind-hindered sites were considered 'direction hindered' if they ranked high for directional divergence (with winds consistently blowing away from climate analogues) and 'speed hindered' if they had a low directional divergence. Directional divergence was measured as the product of windshed anisotropy (calculated as one minus the circular standard deviation of the bearings to all cells in a site's 500-km-diameter landscape, weighted by their wind accessibility) and divergence angle (calculated as the angle between bearings to the centroids of the windshed and climate surfaces, with centroids defined as the weighted mean coordinates of all the cells in a site's 500-km-diameter landscape, weighted by accessibility or climate similarity).

***P. contorta* case study.** To model how wind patterns are predicted to shape genetic rescue and species range expansion in lodgepole pine, we transferred an expert range map that represents the current distribution⁵⁹ to the CFSR raster grid. For the gene flow analysis, to model the genetic rescue potential for a given population in the species range, we calculated both upwind accessibility and inbound climate similarity to every other cell in the range, and then summed the product of these two values across all cells in the species range. This process was repeated for every grid cell in the species range. To calculate the climatic similarity, the mean annual temperature was used with a niche standard deviation of 2°C , to approximately

match the estimated thermal niche breadth of individual populations of *P. contorta*^{52,53,60}.

To model the species range expansion, we fitted a MaxEnt climatic niche model⁶¹ based on the 12 temperature and precipitation variables listed above, using the species current range as presences and the surrounding region as background. We then estimated future climatic suitability by projecting the model using future climate data. To estimate the wind-dispersal potential outside the current range, we generated a region-wide downwind accessibility surface for every grid cell in the current range and took the sum of these surfaces to represent the estimated dispersal shadow of the entire species range. We used a quadratic wind conductance function because the dispersal of heavier seeds often exhibits exponential relationships with windspeed as described in Supplementary Appendix 1. The summed wind-shadow surface was multiplied by the climatic suitability surface to identify areas outside the current range that are predicted to be both suitable and accessible.

CMIP5 analysis. To assess the long-term stability of prevailing winds over periods of climate change, we compared wind between the Last Glacial Maximum, twentieth century and late twenty-first century, based on general circulation model simulations⁶². To derive wind climatologies for an ensemble of four CMIP5 models that had simulations available for all three time periods (CNRM-CM5, IPSL-CM5A-LR, MIROC-ESM and MRI-CGCM3), we calculated mean u and v windspeeds across years for each model run, averaged these across runs for each model and finally averaged these across models to derive a final ensemble mean. Both u and v values were then compared across time periods for each grid cell.

R code. All data analysis was done in R version 3.5.1⁶³. The code is available online^{64,65}.

Data availability

All the input data used in the study are publicly available. Source data that represent the results associated with each figure accompanies this paper.

Code availability

All R code used in the analysis has been deposited in the Zenodo data repository (<https://doi.org/10.5281/zenodo.3860687>)⁶⁴, as has the source code for the version of the windscape R package developed and used for this study (<https://doi.org/10.5281/zenodo.3857730>)⁶⁵.

References

54. Karger, D. N. et al. Climatologies at high resolution for the Earth's land surface areas. *Sci. Data* **4**, 170122 (2017).
55. Dobrowski, S. Z. et al. The climate velocity of the contiguous United States during the 20th century. *Glob. Change Biol.* **19**, 241–251 (2013).
56. van Etten, J. R. Package gdistance: distances and routes on geographical grids. *J. Stat. Softw.* **76**, 1–21 (2017).
57. IPCC Special Report on Global Warming of 1.5 °C (eds Masson-Delmotte, V. et al.) (WMO, 2018).
58. Schleussner, C. F. et al. Differential climate impacts for policy-relevant limits to global warming: the case of 1.5 °C and 2 °C. *Earth Syst. Dyn.* **7**, 327–351 (2016).
59. Little, E. L. Jr *Atlas of United States Trees. Volume 1, Conifers and Important Hardwoods* Miscellaneous Publication 1146 (US Department of Agriculture, 1971).
60. Wang, T., Hamann, A., Yanchuk, A., O'Neill, G. A. & Aitken, S. N. Use of response functions in selecting lodgepole pine populations for future climates. *Glob. Change Biol.* **12**, 2404–2416 (2006).
61. Phillips, S. J., Anderson, R. P. & Schapire, R. E. Maximum entropy modeling of species geographic distributions. *Ecol. Model.* **190**, 231–259 (2006).
62. Taylor, K. E., Stouffer, R. J. & Meehl, G. A. An overview of CMIP5 and the experiment design. *Bull. Am. Meteorol. Soc.* **93**, 485–498 (2012).
63. R Core Team (2017). *R: A Language and Environment for Statistical Computing* (R Foundation for Statistical Computing, 2017); <https://www.R-project.org/>
64. Kling, M. M. & Ackery, D. D. *Scripts and Data used in 'Global Wind Patterns and the Vulnerability of Wind-Dispersed Species to Climate Change'* (Zenodo Repository, 2020); <https://doi.org/10.5281/zenodo.3860687>
65. Kling, M. M. *Windscape R Package v1.0.0* (Zenodo Repository, 2020); <https://doi.org/10.5281/zenodo.3857730>

Acknowledgements

M.K. was funded by a US National Science Foundation Graduate Research Fellowship. We thank B. Collins for providing access to wind data from CMIP5 simulations.

Author contributions

M.K. conceived the study, conducted the analyses and drafted the manuscript. D.A. contributed discussion and feedback on the study design and edited the manuscript.

Competing interests

The authors declare no competing interests.

Additional information

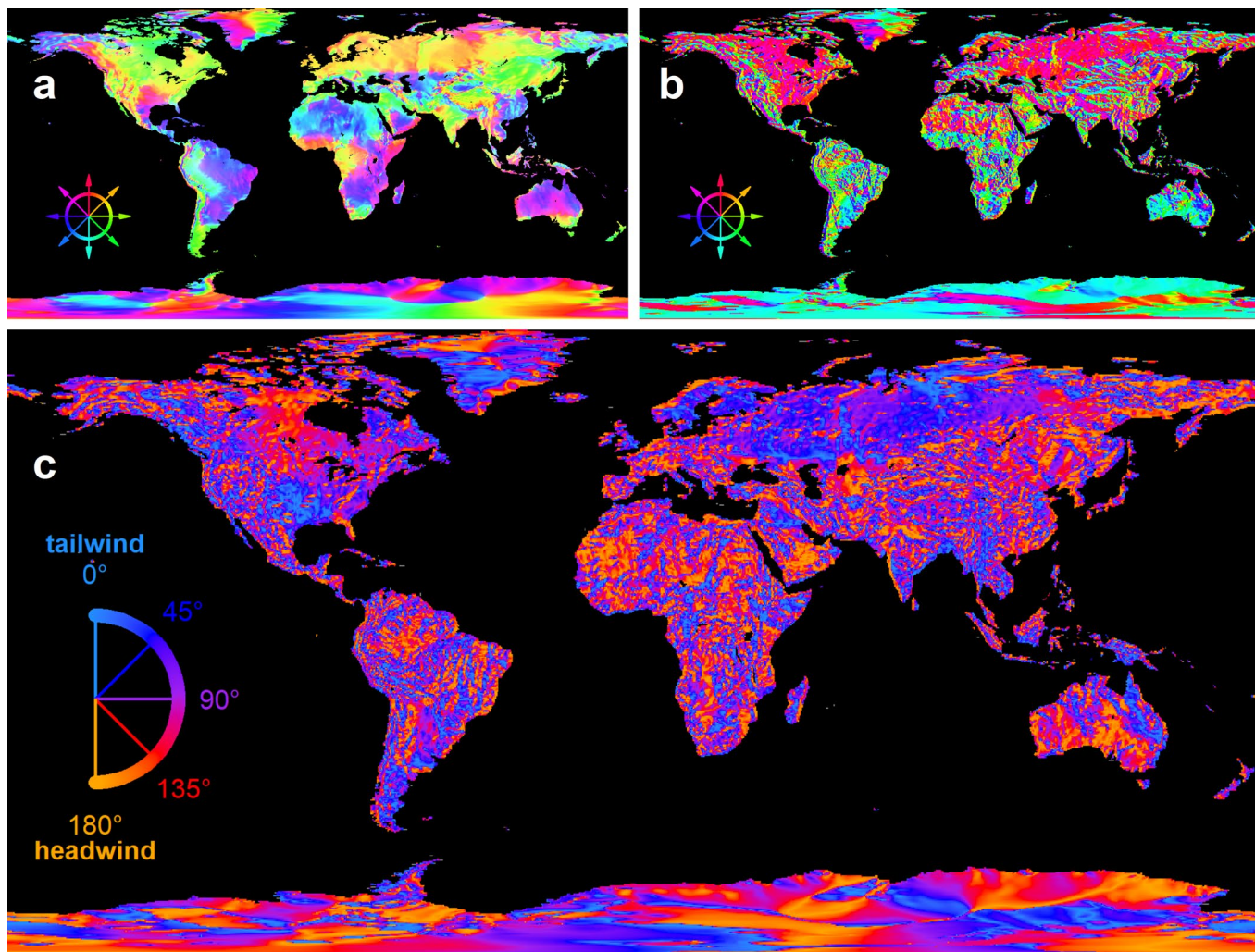
Extended data is available for this paper at <https://doi.org/10.1038/s41558-020-0848-3>.

Supplementary information is available for this paper at <https://doi.org/10.1038/s41558-020-0848-3>.

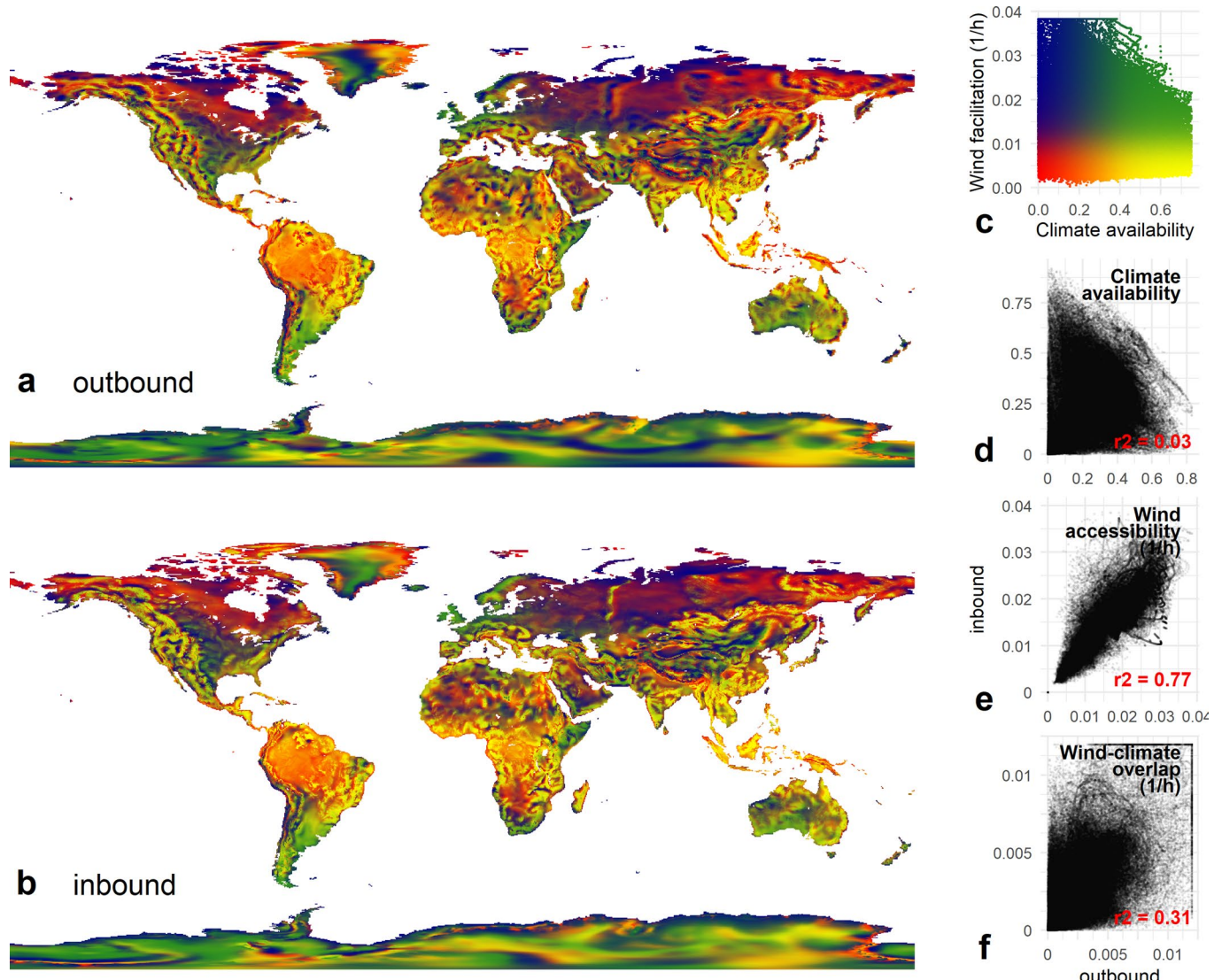
Correspondence and requests for materials should be addressed to M.M.K.

Peer review information *Nature Climate Change* thanks Gil Bohrer, Frank Schurr and the other, anonymous, reviewer(s) for their contribution to the peer review of this work.

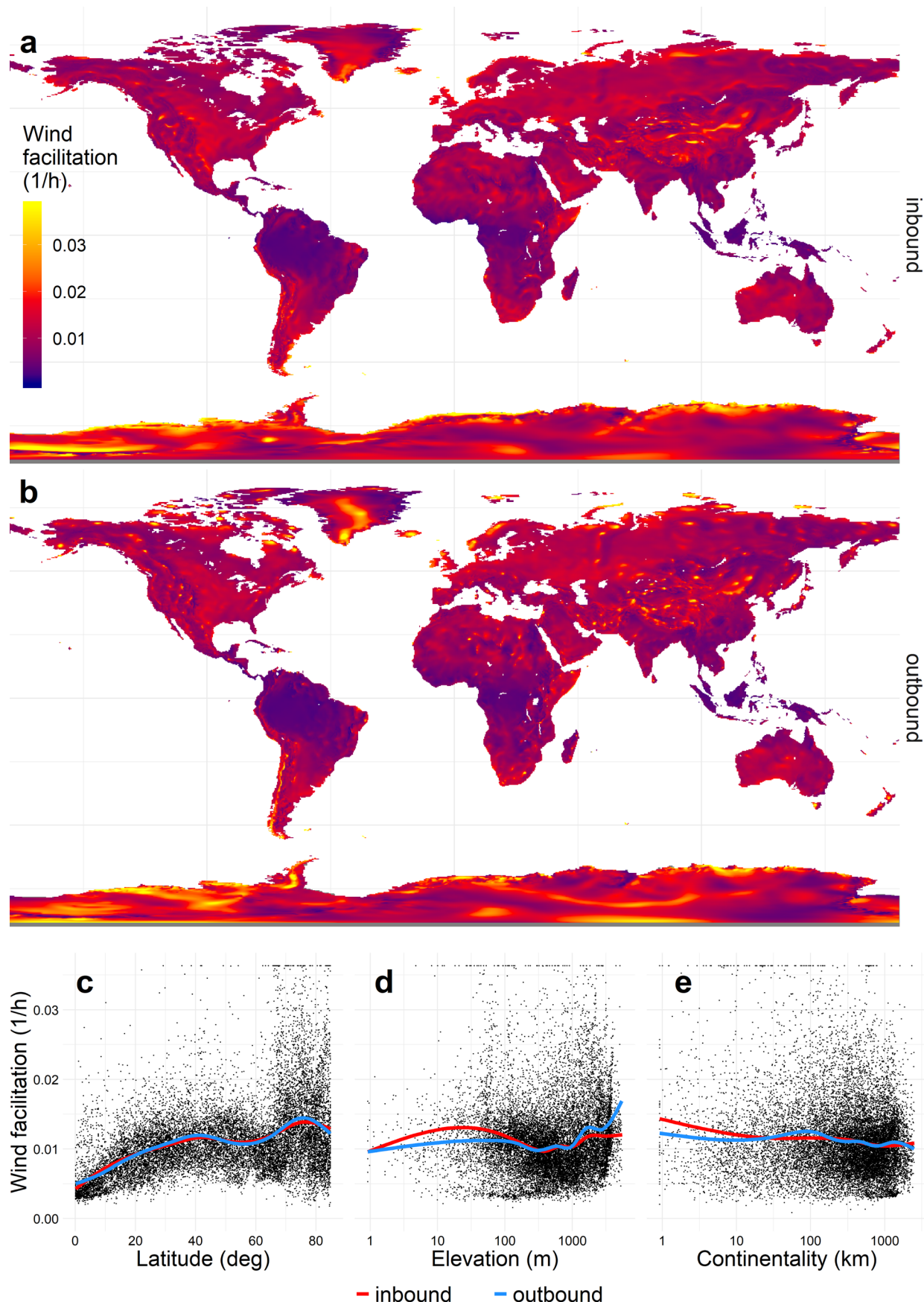
Reprints and permissions information is available at www.nature.com/reprints.



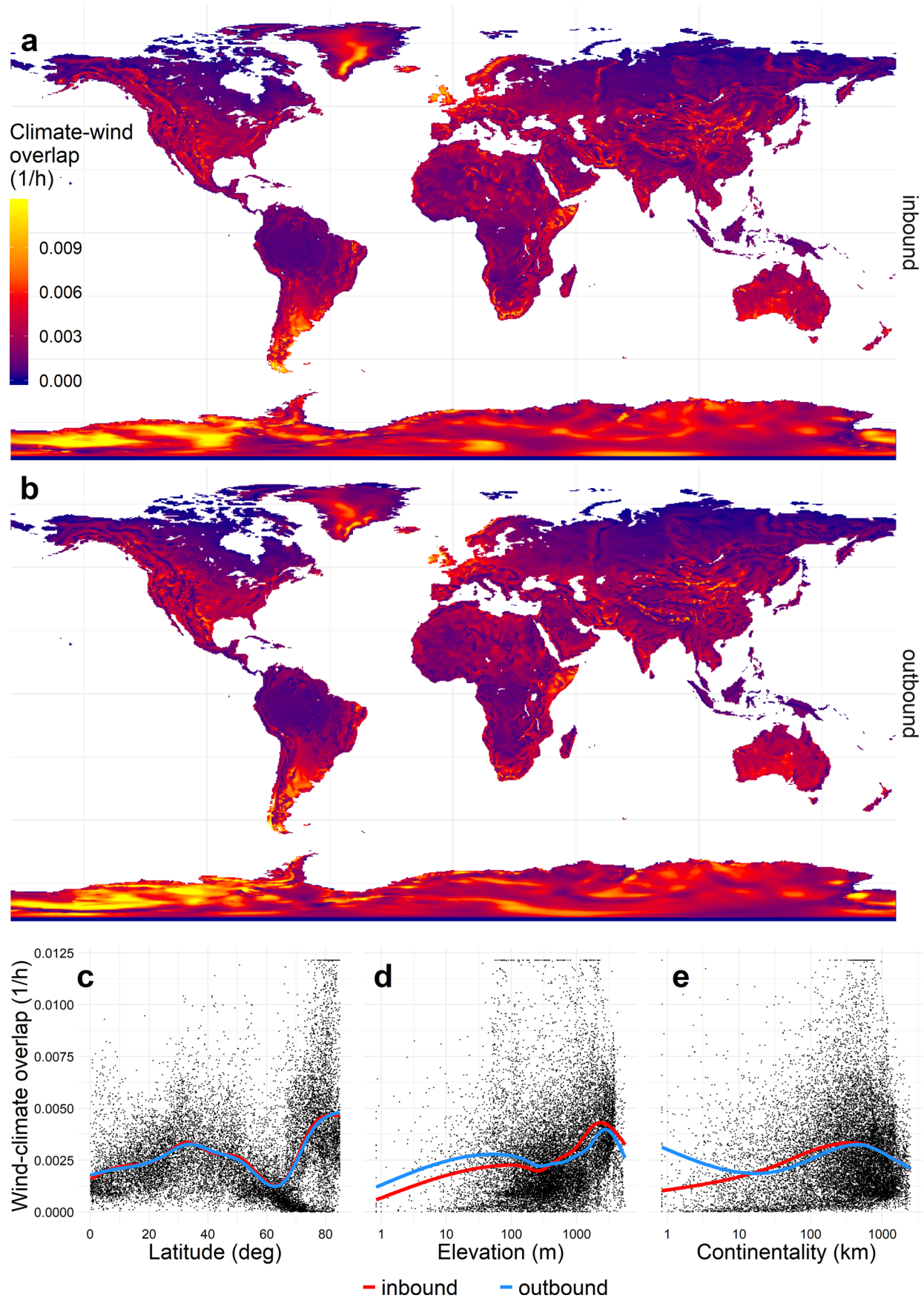
Extended Data Fig. 1 | Global patterns of alignment between prevailing wind direction and temperature gradients. **a**, Prevailing local wind direction, that is the bearing at which wind-dispersed organisms are expected to move on average. **b**, Direction of temperature gradient descent, that is the local direction in which organisms will need to move to offset warming climate. **c**, The difference between these two directions, with 0° indicating migratory tailwinds (prevailing winds blow directly down the temperature gradient) and 180° indicating migratory headwinds (prevailing winds blow directly up the temperature gradient).



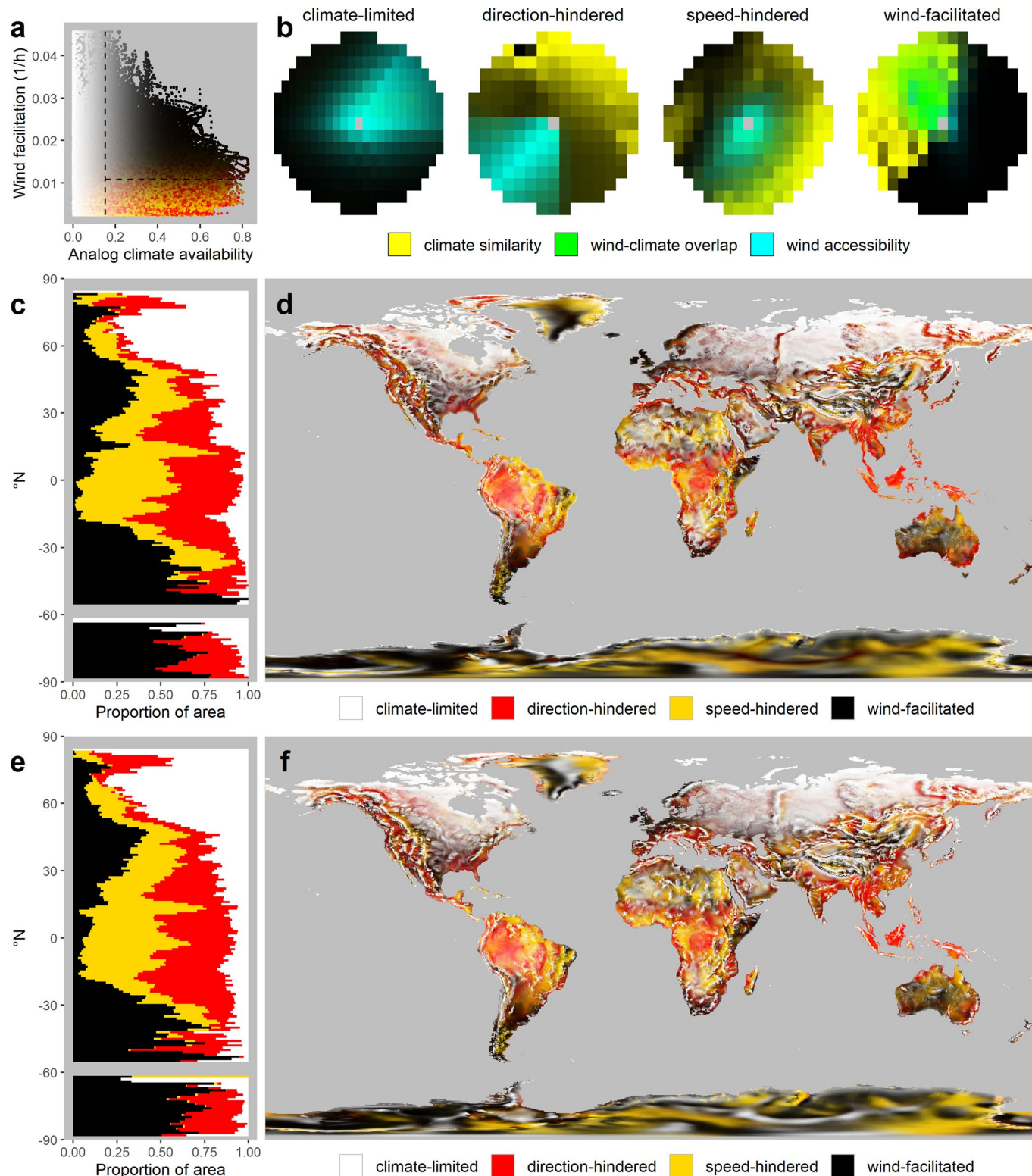
Extended Data Fig. 2 | Global patterns of landscape overlap between windsheds and climate analogs. Maps show the amount of climatically analogous area versus the proportion of that area that is wind-accessible within 250 km of each focal site, in the outbound (a), and inbound (b), directions. (Panel a presents the same data as Fig. 4c of the main text, and is repeated here for comparison.) Color represents the bivariate relationship between these variables c, with green and blue indicating wind facilitation and yellow and red indicating wind hindrance. Additional scatterplots (d-f) compare the amount of similar climate, the amount of wind-accessible area, and the amount of wind-climate overlap in the forward versus reverse directions. Extreme outliers are rescaled in panel f for visual purposes only.



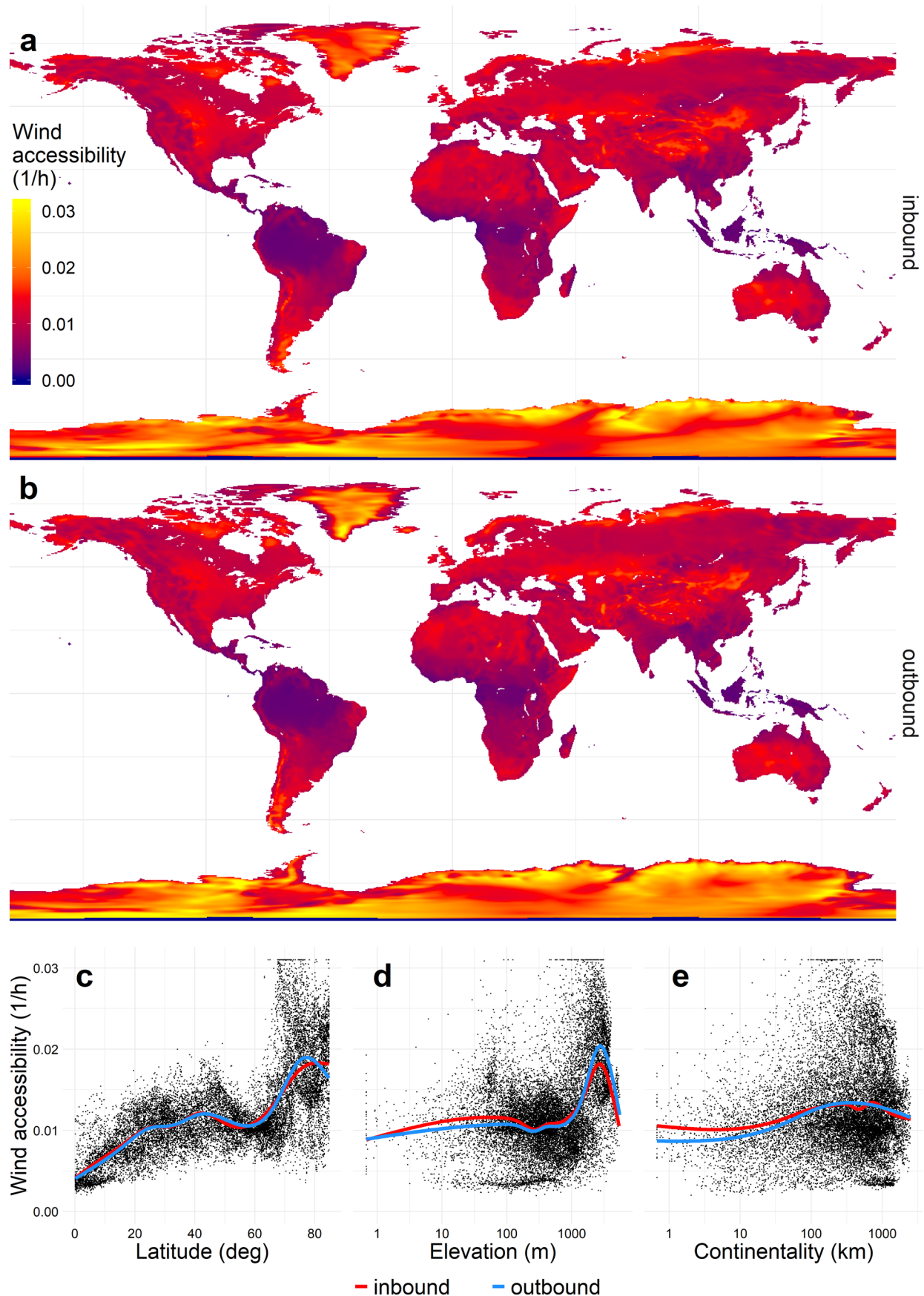
Extended Data Fig. 3 | Global patterns of wind facilitation of climate change tracking. Maps show wind facilitation for the landscape within 250km of each terrestrial grid cell, in the inbound (a), and outbound (b), directions, and with respect to major geographic gradients (c–e). In the scatterplots, latitude represents absolute latitude.



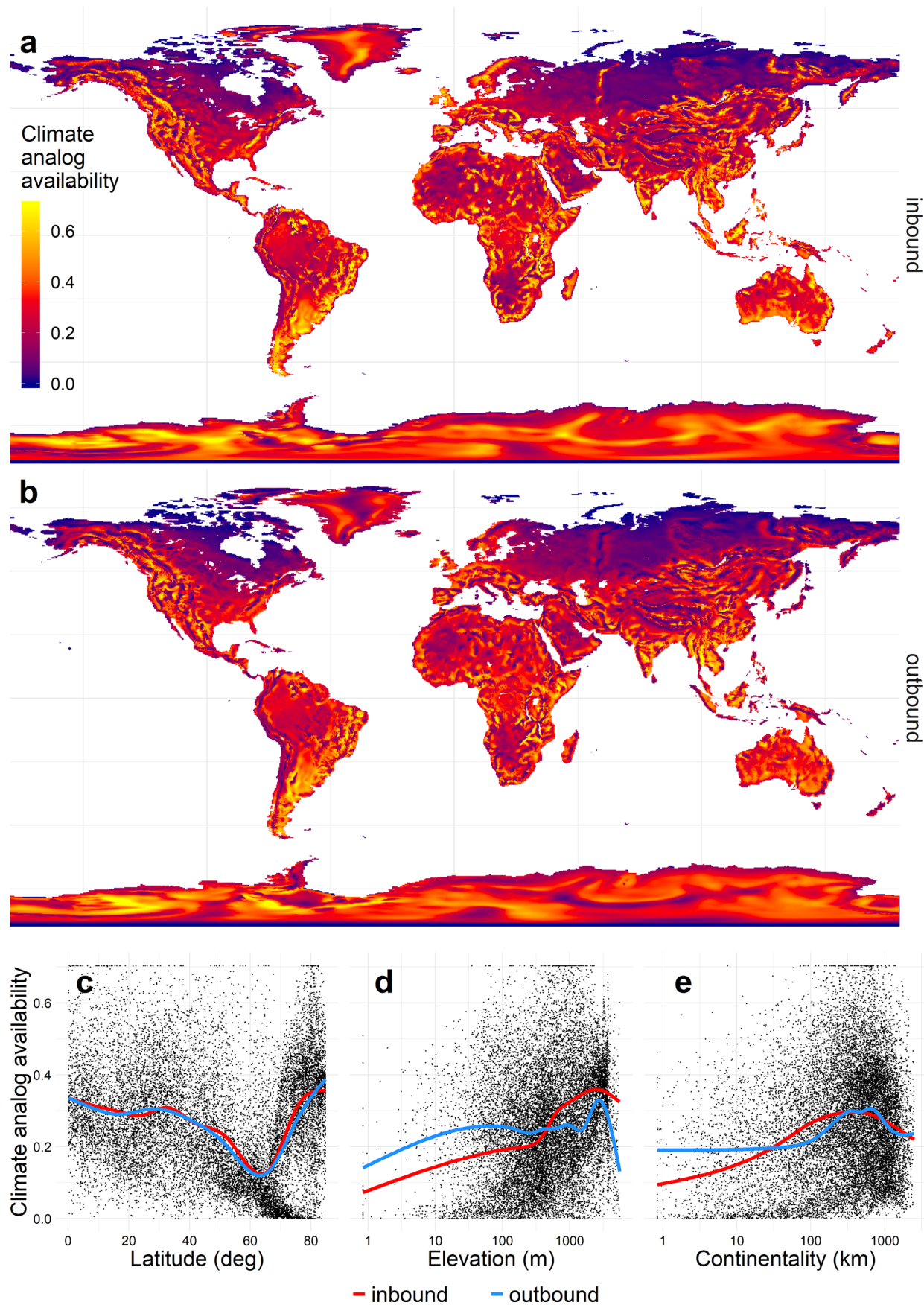
Extended Data Fig. 4 | Global patterns of wind-climate overlap. Maps show overlap for the landscape within 250km of each terrestrial grid cell, in the inbound (a), and outbound (b), directions, and with respect to major geographic gradients (c–e). In the scatterplots, latitude represents absolute latitude.



Extended Data Fig. 5 | Global patterns of wind facilitation ‘syndromes’. Sites can be assigned continuous rankings or discrete categories representing four alternative syndromes: wind facilitation, directional hindrance, speed hindrance, or climate limitation. **a**, Sites are ranked by climate availability, wind facilitation, and directional alignment (collapsed z-axis differentiating red from yellow) to assign relative membership in each of the four syndromes. **b**, Examples of each syndrome, with colors representing climate similarity, wind accessibility, and their areas of overlap across the 250 km radius landscapes surrounding each central origin cell. **c,e**, Syndrome prevalence by latitude in the inbound and outbound directions, respectively; syndromes are categorized to place 25% of global land area in each category, along the dotted lines depicted in panel **a**. **d,f**, Global map of syndromes in the inbound and outbound directions, respectively, with colors representing a continuous gradient among the four categories as depicted in panel **a**.



Extended Data Fig. 6 | Global patterns of wind accessibility. Maps show the mean wind accessibility of landscapes within 250km of each terrestrial grid cell, in the inbound (a), and outbound (b), directions, and with respect to major geographic gradients (c–e). In the scatterplots, latitude represents absolute latitude.



Extended Data Fig. 7 | Global patterns of climate analog availability. Maps show analog availability within 250km of each terrestrial grid cell, in the inbound (**a**), and outbound (**b**), directions, and with respect to major geographic gradients (**c–e**). In the scatterplots, latitude represents absolute latitude.